The Influence of Structural Characteristics on the Response of Silicon Avalanche Photodiodes to Proton Irradiation

Heidi N. Becker, Tetsuo F. Miyahira, *Member, IEEE*, and Allan H. Johnston, *Fellow, IEEE*

***Abstract*--Different silicon avalanche photodiode structures are compared for the effects of 51-MeV protons on dark current, photocurrent, and noise. Large differences in depletion region volumes contributed to differences in sensitivity to bulk dark current increases. At high fluences, ionization damage appeared to be the dominant mechanism for dark current increases in some devices. Increases in 1/f-type noise and supplemental gamma ray testing indicate that these high dark current increases are due to surface damage effects. A discussion of structural parameters that may heighten radiation sensitivity is presented, including doping levels and p-n junction termination techniques.**

I. INTRODUCTION

THE ongoing interest in space-based light detection and ranging (LIDAR) and optical communications continues to create a demand for highly sensitive and radiation tolerant photodetectors. Avalanche photodiodes (APDs) are often chosen for such systems due to their low noise and high gain compared to conventional detectors. For space applications requiring high sensitivity, radiation-induced changes in device parameters such as dark current need to be quantified so that intensity dependent data are correctly interpreted. Radiation testing of an APD with electrons and gamma rays has been studied by Swanson, et al. [1]. However, radiation effects on differing avalanche photodiode structures have not been widely presented. This study examines three different silicon avalanche photodiode structures: conventional APDs from Advanced Photonix and Pacific Silicon Sensor, and an IR-enhanced APD from Perkin Elmer.

Fig. 1 shows a typical APD structure and the processes that occur in different regions of the device. Other device configurations are possible, but the basic principles are the same. APDs use a reverse bias applied to a p-n junction. They operate in a fully depleted mode in that the reverse bias creates a depletion region in the diode that extends all the way from the junction to the p+ region at the other side of the device. Light is absorbed and creates electron-hole pairs in the depletion region. Electrons are swept via drift toward a very high field region at the p-n junction called the avalanche (multiplication) region. It is here that the electrons become energetic enough to create additional electron-hole pairs by impact ionization, starting a chain reaction where additional electron-hole pairs are created. Avalanche multiplication is the internal gain mechanism of APDs.

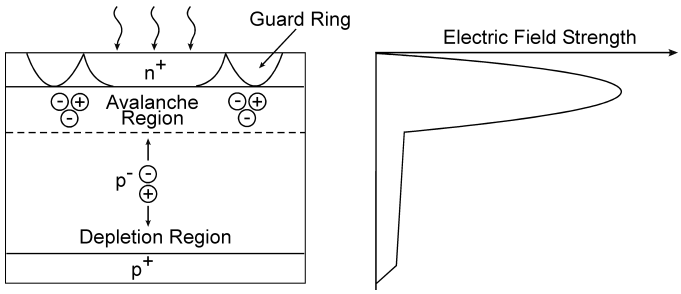

Fig. 1 Schematic of the avalanche process in an APD

Dark current in APDs has two components: surface currents which are unaffected by gain, and bulk leakage current which passes through the avalanche region and is therefore gain multiplied. A common approach to controlling surface current is the incorporation of one or more guard rings [2].

II. EXPERIMENTAL PROCEDURE

Three silicon APD structures were studied to determine how 51-MeV proton irradiation affects their characteristics: two "standard" APDs, the 036-70-62-531 by Advanced Photonix (AP) and the AD-800-9 by Pacific Silicon Sensor (PSS), and the RCA Type C30954E IR-enhanced structure by Perkin Elmer (PE). All are high speed APDs with active area diameters of 0.9, 0.8, and 0.8 mm, respectively. However, there are important differences. The PE structure is enhanced for near infrared wavelengths, and has similar responsivity at 800 nm and 1 micrometer. The AP and PSS APDs have more typical responsivity curves, for silicon detectors, which peak near 800 nm and fall off rapidly for longer wavelengths. The IR-enhanced APD has a much larger active collection depth because of the long absorption depth near the silicon bandgap edge. A more complete description of the three structures is presented in Section IV, however Table 1 identifies the dominant characteristic of each APD.

Manuscript received August 22, 2003. This research in this paper was carried out at the Jet Propulsion Laboratory, California Institute of Technology, under contract with the National Aeronautics and Space Administration, Code AE as part of the NASA Electronic Parts and Packaging Program.

The authors are with the Jet Propulsion Laboratory, California Institute of Technology, Pasadena, CA 91109. (telephone: 818-393-5491, e-mail: Heidi.N.Becker@jpl.nasa.gov, Testsuo.F.Miyahira@jpl.nasa.gov, and Allan.H.Johnston@jpl.nasa.gov).

TABLE I
SILICON AVALANCHE PHOTODIODES IN THE STUDY

APD Structure	Depletion Region Depth	Typical Operational Voltage (Gain=100)
Perkin Elmer	Deep (IR-enhanced)	400V
Advanced Photonix	Shallow	200V
Pacific Silicon Sensor	Medium Thickness	200V

The APDs were irradiated up to 10^{12} p/cm^2 at Crocker Nuclear Laboratory, UC Davis using 51-MeV protons. Four to six samples of each structure were irradiated and evaluated under reverse bias, with the voltage required for a pre-irradiation gain of approximately 100. It is important to note that we did not adjust the gain after each dose to match pre-irradiation values, but rather maintained a constant bias throughout testing and characterization that matched operational voltages. This voltage was approximately 400V for the deep IR-enhanced structure, and 200V for the shallow and medium-thickness structures. One to two more parts of each type were irradiated unbiased and tested after each irradiation under reverse bias. Some additional samples were irradiated to 160 krad(Si) with Cobalt-60 gamma rays at the Jet Propulsion Laboratory total dose facility in order to compare proton and gamma radiation effects. The APDs were irradiated at equivalent total dose rates of 100 rad/s (51-MeV protons) and 50 rad/s (gammas). All irradiations were conducted at room temperature, and pre- and post-irradiation characterization was done at 22C using device mounts placed on thermoelectric cooling (TEC) modules. The temperature of the TEC modules was stable to within ± 0.1C. Approximately ten minutes of time passed between irradiation and characterization of the devices. This amount of time was necessary in order for the devices to reach thermal equilibrium with the TEC modules.

In Geiger mode, an APD is operated at a bias above its breakdown voltage, resulting in extremely high gains (as high as 10^6 or more). It is important to note that the data presented in this study relate to the case of linear mode operation only, with the APDs biased at voltages below breakdown.

800 nm LEDs were used as a light source for cw photocurrent measurements. 800 nm is near the peak of the responsivity curves for these detectors and close to 815 nm, a water absorption line that is important for certain LIDAR atmospheric studies [3]. The 800 nm optical power incident on the active areas of the devices was approximately 0.15 microwatts. The entire active area surface was uniformly illuminated; this was accomplished by using opal diffusers between the LEDs and the APD mounts. Three additional samples of the deep IR-enhanced structure were evaluated at 1064 nm following biased proton irradiation, using a diode-pumped cw Nd:YAG laser as the light source. For this light source, an integrating sphere was used in order to illuminate APD active areas uniformly. The 1064 nm optical power incident on active areas was approximately 1.6 microwatts.

Pre- and post-irradiation noise measurements were taken using a special circuit that incorporated a low-noise transimpedance amplifier and was connected to a dynamic signal analyzer. Dark current noise spectral density was evaluated from 10 Hz to 1.6 kHz for the deep and shallow structures irradiated in biased and unbiased conditions. The Pacific Silicon Sensor APD (medium thickness) was not included in the noise study. This was due to the pin out of this APD being different than the Advanced Photonix and Perkin Elmer devices. Our noise circuitry required very short, air-bridged leads in order to reduce stray capacitance, and accommodating the pin out of the Pacific Silicon Sensor device would have required building a second circuit. At the time of this study, funding was not available for a second circuit.

III. EXPERIMENTAL RESULTS

A. Dark Current

Significant increases in dark current (leakage current measured at operational voltages under unilluminated conditions) were observed in all three structures. Fig. 2 shows changes in dark current (ΔI_d) for representative devices of all three structures. Pre-irradiation dark currents were approximately 40 nA (deep) and 1 to 4 nA (shallow and medium). After a fluence of 10^{12} p/cm^2, I_d in most devices was observed to increase by two orders of magnitude above pre-irradiation values. However, post-irradiation I_d was approximately an order of magnitude higher in the deep IR-enhanced structure than in the shallow or medium thickness structures. On a log/log plot there is a linear relationship between dark current increases and fluence.

There was an important exception to this linear trend. Half of the shallow devices irradiated under reverse bias exhibited unusually high shifts in I_d at the higher fluence levels (5×10^{11} and 10^{12} p/cm^2). Post-irradiation I_d was approximately three orders of magnitude above pre-irradiation values for these samples. The response of these devices is also shown in Fig. 2; the circled data points show the departure from linearity of the abnormal samples. This behavior is discussed further in Section IV. It is also important to note the very similar behavior of the shallow and medium thickness devices at lower fluences, since these two structures have quite different depletion region volumes and doping levels. This is expanded upon in Section IV.

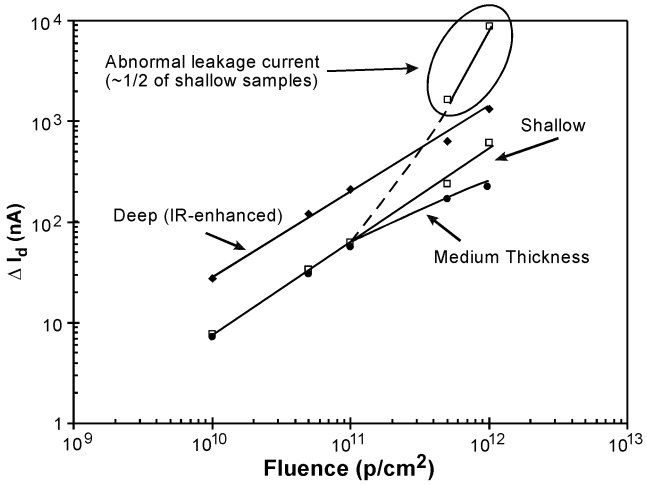

Fig. 2 Changes in dark current from exposure to 51-MeV protons (representative devices irradiated under reverse bias).

Samples of all three structures were irradiated unbiased and tested after each irradiation under bias. Dark current shifts for these parts closely resembled the data for biased irradiations, however no "abnormal" dark current increase was observed at high fluences for the unbiased shallow device.

Measurements following periods of unbiased annealing were taken for up to six days following irradiation (unbiased annealing at room temperature was required by project specifications). All three structures maintained much of the high I_d induced by radiation, and changes following the first 48 hours were minimal. Dark current levels for the deep IR-enhanced and medium-thickness devices were still two orders of magnitude above pre-irradiation values following the annealing period (Fig. 3). The more well-behaved samples of the shallow structure also retained an I_d that was two orders of magnitude above pre-irradiation levels. Although more recovery was observed in the "abnormal" shallow devices, the dark current levels were still three orders of magnitude above pre-irradiation levels after annealing.

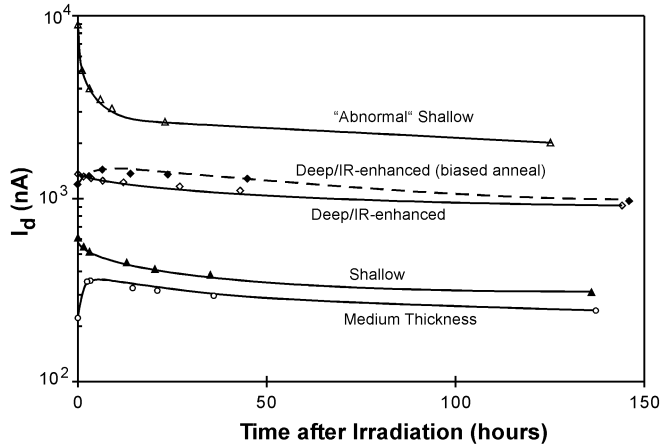

Fig. 3 Dark current annealing data for representative devices irradiated under reverse bias with 51-MeV protons and annealed unbiased at room temperature (one exception noted).

One deep device was annealed under bias at room temperature using the voltage that was required for a pre-irradiation gain of 100. An unusual "reverse annealing" effect was observed with this device. Several hours following irradiation, I_d was 20 percent higher than it had been immediately following irradiation. After the initial increase, the dark current slowly decreased, reaching a level 20 percent below the post-irradiation value by the sixth day of annealing. One of the deep devices that was annealed unbiased exhibited the same behavior. Although this effect is not understood, a similar effect was reported by Swanson et al. [1], who observed a 33 percent increase in I_d 28 minutes after irradiation in APDs tested with electrons and gamma radiation.

Reverse annealing was also observed with all samples of the medium-thickness devices. However, I_d levels following the annealing period never dropped below the post-irradiation value with this structure.

B. Photocurrent

Photocurrent changes at 800 nm are presented in Fig. 4 for representative devices. The photocurrent of all structures decreased consistently with fluence. Losses by 10^{12} p/cm^2 were approximately 65 percent (deep and medium) and 50 percent (shallow). Data taken at 1064 nm with the deep (IR-enhanced) structure is also presented. Note that losses at 1064 nm were twice as severe than at 800 nm for this structure. Results for unbiased irradiations were similar, however, at higher fluences, unbiased irradiations yielded photocurrent losses that were 10 to 20 percent less than with biased irradiations.

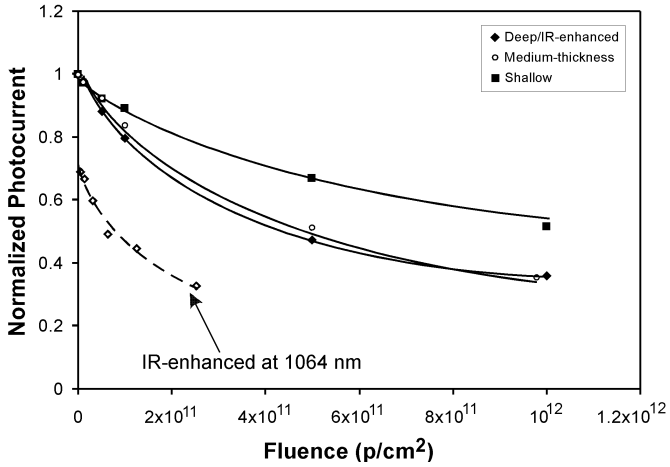

Fig. 4 Changes in photocurrent from exposure to 51-MeV protons (representative devices irradiated under reverse bias).

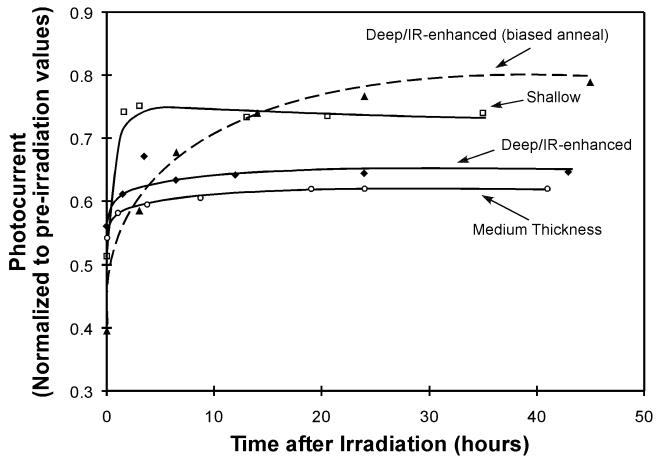

Fig. 5 Photocurrent annealing data for representative devices exposed to 51-MeV protons (biased irradiations).

Fig. 5 presents photocurrent recovery data for representative devices. After approximately two days of unbiased annealing at room temperature, photocurrent losses were about 25 percent (shallow), 32 percent (medium), and 35 percent (deep) compared to pre-irradiation values. Most of this recovery occurred within the first few hours of annealing. The deep device that was annealed under bias showed greater recovery, having only a 20 percent loss of photocurrent after 45 hours of annealing. Its recovery was also more gradual compared to the unbiased annealing data. Recovery for unbiased irradiations was 2 to 5 percent less than for biased irradiations.

All devices in the study were irradiated with their TO-5 packaging and cover glass intact. It is unlikely that the presence of the glass is influencing our data, since irradiation with Co-60 yielded no photocurrent changes in the devices.

C. Noise

Our three APD structures have specified dark current noise spectral densities of 0.4 to 2 $pA/Hz^{1/2}$ at 10 kHz. Noise spectra from 10 Hz to 1 kHz were evaluated before and after irradiation with 51-MeV protons and Co-60 for deep and shallow samples. This measurement bandwidth was chosen to emphasize changes in 1/f-type noise. Fig. 6 shows data for a shallow structure taken prior to irradiation, following biased irradiation with protons, and after one week of annealing. Data from another shallow device following biased irradiation with gammas is also included. Power line harmonics are evident in initial measurements, but disappear after the noise increases from radiation damage. After 10^{12} p/cm^2, dark current noise across our measurement spectrum increased by approximately one decade. There was a slightly higher increase in the lower frequency (1/f) component of the noise. Although all noise components exhibited annealing, there was less annealing at higher frequencies.

The Co-60 data is noticeably different than the proton data. There was a very high increase in 1/f noise following gamma radiation, and a much smaller increase in high frequency noise. It is important to note that post-irradiation DC dark current was almost 50 percent greater in the sample irradiated with Co-60. Since we have shown that the shallow structure exhibits different behavior on a part-to-part basis, what is important to appreciate is not the relative noise amplitudes, but rather the relative slopes of the noise spectra. Swanson et al. [1] observed similar increases in 1/f noise in an APD biased for a gain of 100 and irradiated with 1.5-MeV electrons to 300 krad (Si). They attributed increases in high frequency noise to increases in bulk damage and gain-multiplied dark current. Increased 1/f noise was linked to increased surface leakage currents, most likely caused by trapped holes in the oxide layer creating an n-type channel in the lightly doped p-region of their structure.

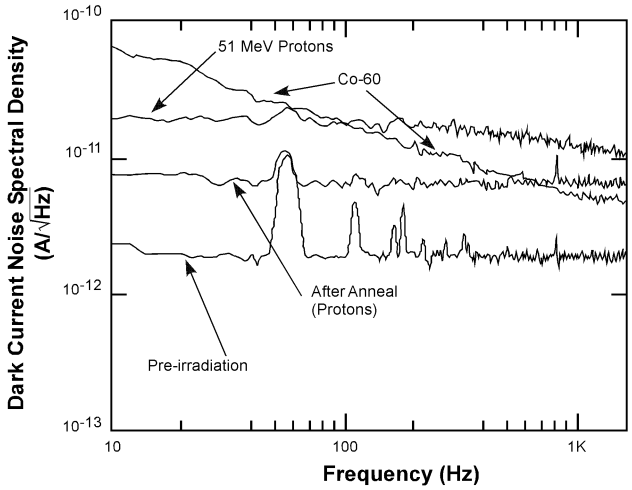

Fig. 6 Noise results for the Advanced Photonix (shallow) structure after irradiation to 10^{12} p/cm^2 or 160 krad(Si) [equivalent total dose].

Increases in noise were smaller (about a factor of 2 less) and relatively flat across the measurement spectrum for unbiased irradiation. Several devices (both shallow and deep) that had increases in dark current of 1 microampere or more, saturated our noise measurement circuitry, so comparison of the data from typical and "abnormal" shallow devices is not possible.

The deep structure irradiated with protons showed smaller noise increases than the shallow structure. The noise spectrum was relatively flat following irradiation and was approximately 10 $pA/Hz^{1/2}$ at all frequencies. After one week of annealing the spectrum was still flat but had decreased to approximately 8 $pA/Hz^{1/2}$. Results were similar for unbiased irradiations. The results from Co-60 testing of the deep structure were marred by the same saturation issue reported above.

IV. Analysis and Discussion

A. Structural Differences in the APDs

Spreading resistance measurements were used to determine the doping profiles of the three APD structures (Fig.'s 7 to 9). Table 2 lists key structural parameters of the depletion regions of each device.

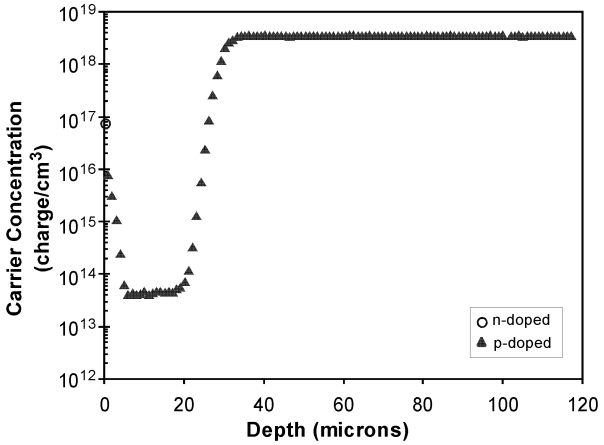

Fig.7 Doping profile of shallow Advanced Photonix APD

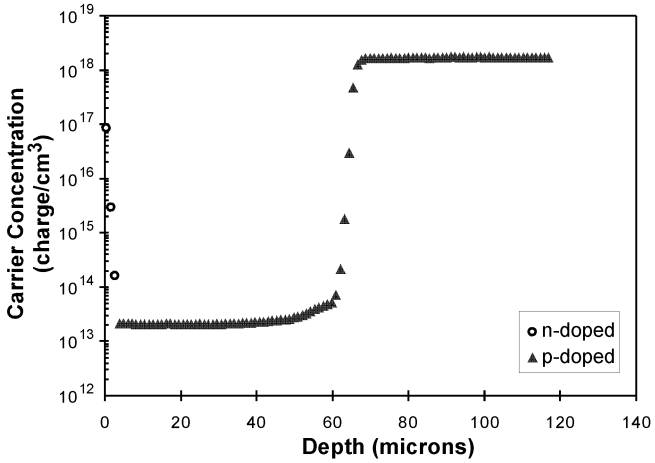

Fig. 8 Doping profile of medium-thickness Pacific Silicon APD

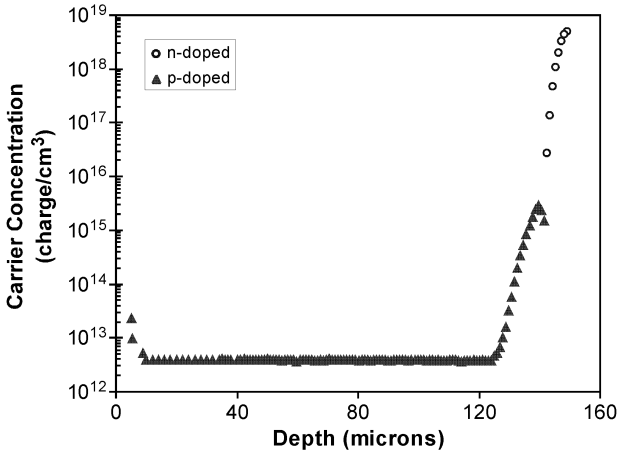

Fig. 9 Doping profile of deep (IR-enhanced) Perkin Elmer APD

TABLE II
APD DEPLETION REGION CHARACTERISTICS

APD Structure	Depth (microns)	Volume (cm^3)	Carrier Concentration (cm^{-3})	Resistivity (Ohm-cm)
Perkin Elmer IR-enhanced (deep)	130	6.5×10^{-5}	4×10^{12}	3400
Pacific Silicon (medium thickness)	60	3×10^{-5}	2×10^{13}	600
Advanced Photonix (shallow)	25	1.3×10^{-5}	4×10^{13}	300

The lightly doped, near intrinsic region of the Perkin Elmer APD is approximately 130 microns deep, twice the depth of the medium-thickness Pacific Silicon APD and five times that of the shallow Advanced Photonix APD. This difference can be explained because the Perkin Elmer device is enhanced for wavelengths up to approximately 1 micron. Since the 1/e absorption depth of photons at 1 micron in silicon is over 200 microns (compared to approximately 15 microns at 800 nm), a depletion region approaching this depth is necessary to achieve efficiency at long wavelengths [2]. Since the APD structures were deliberately chosen so as to have similar active region areas, the depletion region volumes for the three structures scale approximately with depth. Note also that the carrier concentration of the i-region of the Perkin Elmer device is very low (4×10^{12} cm^{-3}) and approximately an order of magnitude less than the other two devices.

B. Commentary Regarding Photocurrent Losses

Changes in responsivity are expected for conventional photodiodes where diffusion (and hence minority carrier lifetime) contribute to charge collection. However, because APDs operate in a fully depleted mode with carriers being transported via drift, we do not believe that we can legitimately correlate photocurrent degradation to the familiar mechanism of reduced minority carrier lifetime from displacement damage [4], [5]. The field in the p- depletion region is high enough that carrier velocities approach saturation, which makes carrier transit times as low as 2 nanoseconds or less [6].

As stated earlier, project requirements dictated experimentation with a constant bias, not a constant gain. We have deliberately not referred to “responsivity” losses, but rather “photocurrent” losses, because responsivity is gain dependent in APDs. What we may be observing is a radiation mechanism where displacement damage changes the electric field distribution within the diode causing a change in the effective gain or in the multiplication probabilities in different regions of the p- layer [7]. This is an area of ongoing investigation. However, unless losses were extreme, the magnitude of an APD’s signal in many applications may be relatively unimportant, especially if internal calibration is part of the system in question.

C. Volume Dependence of Bulk Dark Current Increases

Our data show irradiation from 51-MeV protons causing dark current increases of two orders of magnitude after 10^{12} p/cm^2 in the three silicon APDs studied. Kalma and Hardwick [8] observed similar dark current changes in fully depleted silicon PIN diodes after irradiation with 1-MeV neutrons. Because APDs operate in a fully depleted mode, this is an appropriate comparison. Previously, leakage current increases in neutron irradiated silicon devices have been attributed primarily to the creation of carrier generation centers in the depletion region bulk by displacement damage. Our data agrees well with calculations of dark current changes (ΔI_d) based on the displacement damage coefficients for silicon depletion regions of Srour, et al. [9] according to

$$\frac{\Delta I_d}{V} = \frac{q n_i \phi}{2 K_{gn}} \qquad (1)$$

where V is the depletion region volume, n_i is the intrinsic carrier density, ϕ is the neutron fluence, and K_{gn} is the damage coefficient. Bulk dominated dark current can also be considered to be gain multiplied. After applying the appropriate NIEL ratio [10], [11] and correcting for APD gain, our $\frac{\Delta I_d}{V}$ from 51-MeV protons are within a factor of 2 of that reported by Kalma and Hardwick in silicon PIN diodes after neutron irradiation (one exception was that the medium thickness structure was a factor of 4 less at 10^{12} p/cm^2).

As is evident from (1), ΔI_d from displacement damage is directly proportional to depletion region volume. It is evident from our data that displacement damage is contributing to the observed dark current increases in our three structures. However, displacement damage considerations alone are not sufficient to explain the observed behaviors of the structures.

The depth of the medium-thickness APD is twice that of the shallow APD. However, a factor of two difference in ΔI_d was not observed. In fact, the behavior of the two structures was virtually the same at lower fluences. A general guideline for bulk leakage current sensitivity cannot be reduced to volume considerations alone. The shallow structure has a carrier concentration that is twice that of the medium-thickness structure. Although damage constants for very high resistivity Si are not as widely known, damage coefficients for lower resistivity Si tend to increase with carrier concentration [12]. The medium-thickness device may be showing less damage than expected due to having a lower carrier concentration in the p- layer than the shallow device. In other words, the difference in volume of the medium and shallow structures may be offset by the differences in their carrier concentrations.

The depletion region volume of the deep APD is 5 times greater than the shallow APD. Although the respective changes in dark current have a ratio close to 5 to 1 at lower fluences, this ratio decreases to approximately 2 to 1 by 10^{12} p/cm^2. In addition, the "anomalous" shallow devices, whose dark current changes far exceed those of the deep devices at higher fluences, change this ratio at 10^{12} p/cm^2 to *1 to 7*! It is evident that another mechanism is responsible for the high leakage currents in the shallow structure.

D. Effect of Ionization on Surface Dark Current Increases

Supplemental testing with Co-60 was performed to determine the total ionizing dose (TID) contribution to the dark current changes observed with protons. Although both types of radiation cause ionization damage, gamma radiation primarily causes ionization with minimal displacement damage, while protons produce both ionization and displacement effects.

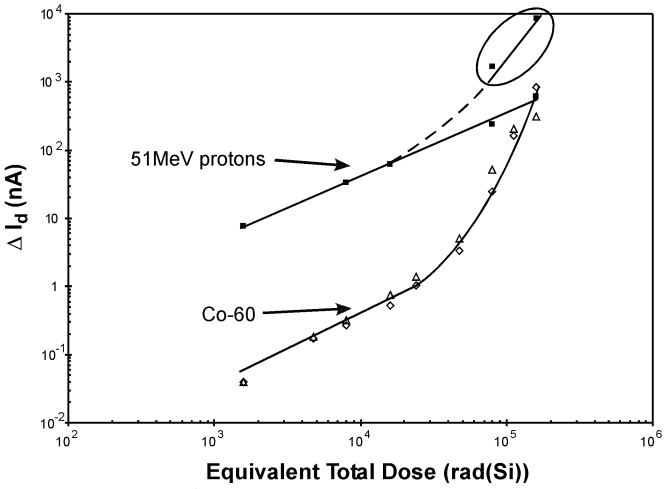

Fig. 10 Comparison of changes in Dark Current due to 51-MeV protons and Co-60 (shallow Advanced Photonix APD)

Fig. 10 revisits the 51-MeV proton data for the shallow structure and includes data from gamma radiation testing of this structure. At lower equivalent total dose levels, gamma radiation yielded a relationship between damage and dose that was similar to that of the 51-MeV proton results. The proton and gamma plots also appear to be approximately separated by the expected NIEL ratio for displacement damage from 51-MeV protons compared to gamma-induced Compton electrons. This indicates that displacement damage (bulk damage) was the major radiation effect observed with protons at lower fluences and that ionization (surface effects) was far lower. At the higher dose levels, gamma radiation also caused a more rapid increase in dark current, with the "knee" in the data occurring at the same level of approximately 25 krad(Si). Dark current increases were not quite as high as what was observed with protons at higher dose levels. However, gamma testing was done with devices from a different lot than that

used for proton testing, and lot-to-lot part variation may be responsible for this difference.

Isochronal annealing was performed on representative proton-irradiated samples of the three structures, including one "abnormal" shallow device (see Fig. 11). Devices were placed in a nitrogen-purged oven for 30 minute periods before being recharacterized. The temperature for the first period was 80 C, and was increased by 20 C for each subsequent period. This technique was chosen in the event there was a temperature threshold for annealing (which did not prove to be the case). The maximum temperature used for the shallow and medium thickness devices was 100 C, because the maximum storage temperature was 85 C for the shallow parts and unknown for the medium thickness parts.

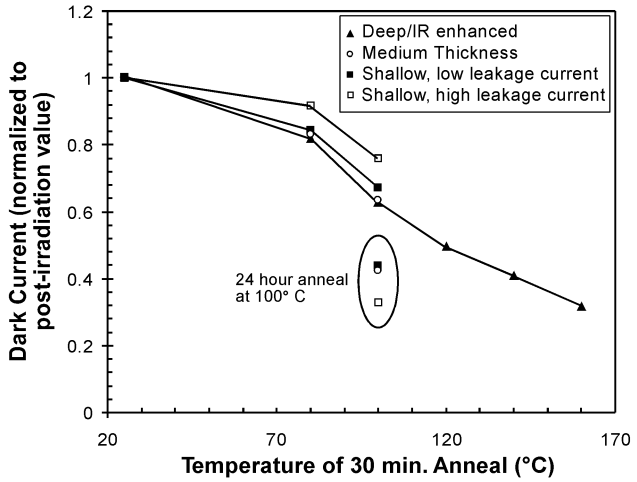

Fig. 11 Isochronal anneal of APDs irradiated under bias with 51-MeV protons

A gradual reduction in dark current was observed in all our structures during isochronal annealing. However, very little change in photocurrent was observed at any temperature. Although data for temperatures above 100 C is not available for the shallow and medium thickness structures, the recovery rates for the three structures appear similar at 100 C and below.

After the initial 30 minutes at 100 C, the shallow and medium thickness devices underwent a 24-hour anneal at 100 C. A 57 percent reduction in dark current was observed in these devices following the 24-hour anneal. Similar reductions may also have occurred in the deep (IR-enhanced) device at 100 C if the annealing periods for this device had been longer than 30 minutes. The abnormal shallow device showed the largest reduction in I_d, losing 67 percent after the 24-hour anneal. This is a further indication that surface damage (ionization) was a greater issue for the "abnormal" shallow devices, as this type of damage tends to anneal more readily with temperature than displacement damage [13].

Our supplemental testing with gamma radiation suggests that a TID effect is a significant contributor to the dark current in the shallow structure, especially at equivalent total doses above 25 krad(Si). The increase in 1/f noise observed after irradiation with the shallow structure also suggests that surface effects are very important [1]. This effect also seems to have both a lot-to-lot and part-to-part variability. The shallow structure uses four guard rings to control leakage current along the junction edges caused by the junction curvature effect. Previous work with high voltage power MOSFETs [14] has shown that charge trapping in the oxide above and between field rings can change their effectiveness by inducing n layers in the lightly doped p- region allowing surface currents to flow. Variations or unevenness in the quality of the oxide used for the shallow structure could be leading to the part-to-part variations in radiation response that we observed.

Recall that when the shallow devices were irradiated unbiased no "abnormal" increase in dark current was observed. There also was less of an increase in 1/f-type noise in unbiased shallow devices. This is consistent with the effect of bias on hole trapping in oxide. If irradiations are biased, electrons are swept to the positive contact, leaving the less mobile holes trapped in the oxide. When irradiations are unbiased, electron-hole pairs created during ionization will have more of a tendency to recombine.

The fact that very little increase in dark current was observed with Co-60 until 25 krad(Si) confirms that the increase in dark current following proton irradiation is primarily due to bulk damage at lower fluences. We attribute the relatively small increase in dark current prior to 25 krad(Si) of total dose to displacement damage from Compton electrons produced by gamma ray irradiation.

E. Carrier Removal Concerns

Another concern when choosing an APD is whether carrier removal effects, which become important at higher fluences, may become involved. For example, the depletion region of the deep structure uses a relatively lightly doped p- layer. If carrier removal effects in this region are large enough to cause dopant inversion, turning the p- region into a more neutral layer, then n-type guard rings would lose the ability to control surface leakage currents effectively. Carrier removal has also been shown to cause device failure in solar cells by increasing the resistivity of the base layer to the point where short circuit current abruptly decreases [15]. The change in carrier concentration in p-type silicon as a function of proton fluence is given by:

$$\Delta p = R_c \phi \tag{2}$$

where R_c is the carrier removal rate and ϕ is fluence [16]. Carrier removal rates for 7 to 14 Ohm-cm p-type silicon have been shown to range from 50 to 100 cm^{-1} for 3 and 10-MeV protons [15]. The resistivities of the depletion regions in our APD structures are one to two orders of magnitude higher, and we do not know the exact carrier removal rates for such materials. However, with such low carrier concentrations, one

can assume that carrier removal will eventually become an issue at high enough fluences, possibly leading to APD failure. The contribution of carrier removal effects to our data is an area of continuing study.

F. Selection Considerations

It is evident that care must be used when choosing an APD structure for sensitive space applications. Note that these detectors may be used with light levels as low as several femtowatts and have peak responsivites of 50 to 60 A/W. We observed a ΔI_d of over 1 microamp in the deep (IR-enhanced) structure, and nearly 9 microamps for some shallow samples, after 10^{12} p/cm^2. For space applications requiring light levels near the lower limit of these detectors, shifts in dark current of 1 microamp or more could be quite significant.

At lower fluences there appears to be a relatively straightforward trade off between high responsivity at long wavelengths and sensitivity to bulk damage due to the necessarily long depletion width.

However, the choice of an APD based on bulk damage considerations is further complicated by issues related to the doping level of the depletion region and how these doping levels may influence damage constants. Also, some devices may be inherently sensitive to total dose effects due to the nature of their surface structures. Therefore, device architecture and possible surface effects must also be considered, including the potential for carrier removal effects which can cause type conversion in surface layers thereby weakening the effectiveness of guard rings intended to control leakage currents. We would also caution designers that relative radiation hardness can have a lot-to-lot, or part-to-part variability, as we have shown with the shallow structure.

V. CONCLUSION

There is a continuing need for highly sensitive detectors in space applications. This study examines three avalanche photodiode structures with very different internal structures. Decreased photocurrent and increased dark current were observed after irradiation with 51-MeV protons for all three devices. However, the long-wavelength-enhanced structure with the wider depletion region showed a much larger sensitivity to bulk dark current increases.

Comparison of proton and gamma ray data indicate that radiation-induced increases in dark current are due primarily to displacement damage in the depletion region and are therefore directly proportional to the volume of this region, at low fluences. Because silicon detectors intended for long wavelength applications require wide absorption regions in order to efficiently collect light, there is a trade off between the desire for high gain in the near infrared and sensitivity to bulk damage in the depletion region which leads to increased bulk dark current. For near IR applications, it may be desirable to chose a detector with a smaller depletion region and sacrifice some initial responsivity at wavelengths near 1 micron for the sake of decreasing vulnerability to bulk damage (the importance of dark current increases depends on the application in question). However, our results also show that shallow devices may come with architectural drawbacks that can contribute to surface currents at high enough fluences. It is therefore important to consider volume, doping, and junction termination methods, along with application requirements (such as wavelength and gain), when choosing an APD for use in a radiation environment. We have also shown that part-to-part variability can be significant enough that radiation testing with small sample sizes is not advisable.

VI. ACKNOWLEGMENTS

The authors are indebted to Eric Swanson for very helpful discussions regarding noise measurements. We acknowledge the valuable assistance of Bernard G. Rax in the development of our noise measurement circuitry.

VII. REFERENCES

[1] E. A. Swanson, E. R. Arnau, and F. D. Walther, “Measurements of natural radiation effects in a low noise avalanche photodiode,” *IEEE Trans. on Nucl.. Sci.*, vol. 34, no. 6, pp. 1658-1661, Dec. 1987.

[2] S. M. Sze, *Physics of Semiconductor Devices*, 2nd ed., John Wiley & Sons, 1981.

[3] T. F. Refaat, G. E. Halama, and R. J. DeYoung, “Characterization of advanced avalanche photodiodes for water vapor lidar receivers,” *NASA/TP-2000-210096*, July 2000.

[4] M. Yamaguchi, S. J. Taylor, S. Matsuda, and O. Kawasaki, “Mechanism for the anomalous degradation of Si solar cells induced by high fluence 1MeV electron irradiation,” *Appl. Phys. Lett*., vol. 66, no. 22, pp. 3141-3143, 1996.

[5] M. Yamaguchi, et al., “A detailed model to improve the radiation-resistance of Si space solar cells,” *IEEE Trans. Elec. Dev. Lett.*, vol. 46, no.10, pp. 2133-2137, 1999.

[6] R. P. Webb, R. J. McIntyre, and J. Conradi, “Properties of avalanche photodiodes,” *RCA Rev.*, vol. 35, pp.234-278, 1974.

[7] R. J. McIntyre, “The distribution of gains in uniformly multiplying avalance photodiodes: theory,” *IEEE Trans. Elec. Dev*., vol. ED-19, no. 6, pp. 703-713, 1972.

[8] A. H. Kalma and W. H. Hardwick, “Radiation testing of PIN photodiodes,” *IEEE Trans. on Nucl. Sci*., vol. 25, no. 6, pp. 1483-1488, 1978.

[9] J. R. Srour, S. C. Chen, S. Othmer, and R. A. Hartmann, “Radiation damage coefficients for silicon depletion regions,” *IEEE Trans. on Nucl. Sci.*, vol. 26, no. 6, pp. 4784-4791, 1979.

[10] G. P. Summers, et al., “Correlation of particle-induced displacement damage in silicon,” *IEEE Trans. on Nucl. Sci*., vol. 34, no. 6, pp. 1134-1139, 1987.

[11] G. P. Summers, E. A. Burke, P. Shapiro, S. R. Messenger, and R. J. Walters, “Damage correlations in semiconductors exposed to gamma, electron and proton radiations, *IEEE Trans. on Nucl. Sci*., vol. 40, no. 6, pp. 1372-1379, 1993.

[12] J.R. Srour, S. Othmer, and K.Y. Chiu, “Electron and proton damage coefficients in low-resistivity silicon,” *IEEE Trans. on Nucl. Sci*., vol. 22, no. 6, pp. 2656-2662, 1975.

[13] V.A.J. van Lint, et al., *Mechanisms of Radiation Effects in Electronic Materials*, Vol. 1, John Wiley & Sons, 1980.

[14] R.D. Pugh, A.H. Johnston, and K.F. Galloway, “Characteristics of the breakdown voltage of power MOSFETs after total dose irradiation,” *IEEE Trans. on Nucl. Sci.*, vol. 33, no. 6, pp. 1460-1464, 1986.

[15] M. Yamaguchi, et al., “High-energy and high-fluence proton irradiation effects in silicon solar cells,” *J. Appl. Phys*., vol. 80, no. 9, pp. 4916-4920, 1996.

[16] R. L. Pease, E. W. Enlow and G. L. Dinger, “Comparison of proton and neutron carrier removal rates,” *IEEE Trans on Nucl. Sci*., vol. 34, no. 6, pp. 1140-1146, 1987.